Comparison of global aboveground biomass estimates from satellite obvervations and dynamic global vegetation models

Bassil El Masri[1*], and Jingfeng Xiao[2]

[1] Department of Earth and Environmental Sciences, Murray State University, Murray, KY 42071, USA

[2] Earth Systems Research Center, Institute for the Study of Earth, Oceans, and Space, University of New Hampshire, Durham, NH 03824, USA

Corresponding author: Bassil El Masri (belmasri@murraystate.edu)

Key Points:

- AGB shows the highest variability around the tropical regions among the datasets
- Satellite-based AGB estimates are lower than those simulated by dynamic global vegetation models
- Similar latitudinal trends but large variability in AGB are observed among the datasets

Abstract

The global forest carbon stocks represent the amount of carbon stored in woody vegetation and are important for quantifying the ability of the global forests to sequester atmospheric CO_2 and to provide ecosystem services (e.g., timber) under climate change. The forest ecosystem carbon pool estimates are highly variable and poorly quantified in areas lacking forest inventory estimates. Here, we compare and analyze aboveground biomass (AGB) estimates from five satellite-based global datasets and nine dynamic global vegetation models (DVGMs). We find that across the datasets, mean AGB exhibits the largest variability around the tropical area. Also, AGB shows a similar latitudinal trend but large variability among the datasets. Satellite-based AGB estimates are lower than those simulated by DVGMs. The divergence among the satellite-based AGB estimates can be driven by the methodology, input satellite products, and the forested areas used to estimate AGB. The modeled NPP, autotrophic respiration, and carbon allocation mostly drive the variability of AGB simulated by DGVMs. The future availability of a high-quality global forest area map is anticipated to improve the accuracy of AGB estimates and to reduce the discrepancies among different satellite- and model-based AGB estimates. We suggest that the carbon-modeling community reexamine the methodology used to estimate AGB and forested areas for a more robust global forest carbon stock estimation.

Plain Language Summary

The amount of carbon stored in the forest woody structure is highly variable and not well quantified, despite its importance in the carbon cycle. Here, we compare and analyze aboveground biomass (AGB) estimates from five satellite-based global datasets and nine dynamic global vegetation models (DGVMs). The largest variability in the datasets' mean AGB was around the tropical area. Satellite-based AGB estimates were lower than those simulated by DGVMs. The divergence among the satellite-based AGB estimates can be driven by the methodology, input satellite products, and the forested areas used to estimate AGB. Whereas, the variability of modeled AGB can be related to the carbon sequestration, storage, and respiration parameterization. Future work should reexamine the methodology used to estimate AGB and forested areas for a more robust global forest carbon stock estimation.

1 Introduction

Biomass represents the amount of carbon that ecosystems sequester and store in plant tissues and governs the potential emissions of carbon due to deforestation and wildfire. Accurate delineation

of biomass at different scales is significant for reducing the uncertainties in global carbon flux estimates (Hall et al., 2011). Thus, there is a need to measure carbon stocks in the above- and below-ground compartments of the forest to quantify any changes in these stocks as brought about by human activities and environmental changes.

Numerous studies have demonstrated the importance of quantifying carbon stocks in terrestrial ecosystems (DeFries et al., 2002; Houghton et al., 2009). Forest ecophysiological properties indicate that woody biomass should increase due to increasing atmospheric CO_2 concentrations and this response varies between different forest species (De Kauwe et al., 2015; Norby et al., 2010). This is not surprising given the difficulties in estimating woody biomass at sites and the difficulties in extrapolating the limited woody biomass estimates from local to global scale. Images from active and optical remote sensors can offer the possibility of combining detailed information about the vertical and horizontal structure of the forest (Anderson et al., 2008; Dubayah et al., 2022; Hyde et al., 2005; Lefsky et al., 2002; Popescu, 2007). Data from different satellite sensors can be used to obtain the necessary information needed to estimate forest structure, which is essential for forest monitoring (Dubayah et al., 2000; Hese et al., 2005; Treuhaft et al., 2009). Understanding how the changing climate induces changes in woody biomass is of critical importance to improve our abilities to accurately predict any future changes in the global carbon budget.

Several satellite-based above-ground biomass (AGB) datasets at varying spatial resolutions ranging from 30 m to 1000 m have been developed (Dubayeh et al., 2022; Harris et al., 2021; Hu et al., 2016; Spawn et al., 2020; Santoro et al., 2021; Santoro and Cartus, 2021). These products provide global estimates of AGB for different years. Current AGB data are derived from different methods (e.g., statistical, data-driven) and satellite data (passive and active remote sensors) (Araza et al., 2022; Santoro and Cartus, 2018). This leads to significant differences among the satellite-derived AGB products in terms of total AGB and presents challenges in accurately quantifying the global AGB stocks and estimating the global carbon budget. Uncertainty assessment of AGB products is hindered by the limited availability of in-situ data (e.g., local, national inventories) and by the lack of the accuracy of forested area maps used to produce the AGB estimates. Moreover, the retrieval algorithms can create inaccurate estimates of AGB at the pixel level, resulting in differences in the spatial distribution between the satellite-derived AGB products (Araza et al., 2023). Satellite-based AGB products still provide very

valuable information about global carbon stocks as it is nearly impossible to perform forest inventory globally. A comprehensive quantification of global AGB estimates is needed to gain a better understanding of the variability or consistency among these products.

Dynamic global vegetation models (DVGMs) and terrestrial biosphere models that simulate the carbon, water, and nitrogen cycles can estimate AGB globally typically at coarse spatial resolution (e.g., 0.5^{o}) (Xue et al., 2017; El Masri et al., 2013). Modeled AGB shows high variability and little agreement among models (Ahlström, et al., 2017). This is because of the differences in model structure and parameters associated with vegetation dynamics, productivity, and carbon allocation. Also, the processes that represent land use/land cover change, emissions, and mortality can all lead to biases in AGB (Pugh et al., 2019). However, these models provide a unique opportunity to understand how the changing climate and anthropogenic disturbances induce changes in AGB. Little effort has been dedicated to validating simulated AGB to constrain these models' carbon stock estimates. Thus, evaluating AGB estimates based on DGVMs against satellite-based AGB data is a step toward quantifying model biases and evaluating to what extent these state-of-the-art models can reproduce the magnitude and spatial variability of AGB at regional to global scales.

Here, we provide an evaluation of five satellite-based AGB products and also analyze the global AGB simulations based on an ensemble of nine DGVMs from the TRENDY v10 project (Friedlingstein et al., 2022). The main objective is to compare multiple satellite-derived AGB products and to evaluate the TRNEDY model estimates. We focus on quantifying the regional and spatial variability in AGB among the different datasets and highlighting the differences between the five AGB products and the nine DGVMs. Furthermore, our synthesis analysis quantifies the changes in the global AGB stocks during the past 20 years. This will allow us to identify the regions or areas with the largest change in AGB while providing an intercomparison of the spatial and regional variability in AGB among these products and models.

2 Materials and Methods

2.1 Satellite data

We used five global satellite-based AGB datasets with spatial resolution ranging from 30 m^2 to 1 km^2 for 2000-2020. These datasets include the Harmonized aboveground biomass dataset,

Global Biomass dataset, Global Forest Watch biomass, European Space Agency Climate Change Initiative biomass, and GEDI gridded AGB dataset.

Harmonized aboveground biomass (HAB)

The harmonized aboveground and belowground carbon density (MgC/ha) and AGB standard error (MgC/ha) for the year 2010 were obtained from the Oak Ridge National Laboratory (ORNL)'s Distributed Active Archive Center (DAAC) for Biogeochemical Dynamics website (https://daac.ornl.gov/). The data has a 300 m spatial resolution. HAB AGB includes carbon stored in stems, branches, and leaves (Spawn et al., 2020). This dataset relies on the Global Biomass AGB density data. It is combined with other AGB biomass datasets for Africa and Alaska to address the Global Biomass data emission of small trees and shrubs (Spawn et al. 2020). Grassland AGB was mapped using the normalized difference vegetation index (NDVI), while crop yield was used to estimate cropland AGB (Spawn et al., 2020). The stem volume of living trees was mapped and AGB was estimated from stem volume using wood density and spatialized biomass expansion factor (BEF) estimates (Spawn et al., 2020). Machine learning methods, trained with a plant morphological database from thousands of global field measurements, were used to map the spatialized biomass expansion factors (Spawn et al., 2020).

Global Biomass (GB)

The global biomass AGB (Mg/ha) and standard error (Mg/ha) for 2010 were obtained from the Global Biomass website (https://globbiomass.org). The data has a 100 m spatial resolution. The GB AGB product includes carbon stored in stems, branches, and leaves expressed as oven-dry weight of the woody parts (Santoro et al., 2021). This dataset was produced using a combination of spaceborne optical and synthetic aperture radar (SAR) imagery (Santoro et al., 2021). Radar backscatter datasets from Envisat ASAR and ALOS PALSAR were independently applied to a process-based model, BIOMASAR, to estimate two independent tree stem volumes (Santoro et al., 2021 and references therein). The ASAR living stem volume was mapped at 1000 m spatial resolution and rescaled to 25 m spatial resolution using a linear regression model (Santoro et al., 2021). Then, a moving average window was applied to produce the living stem volume at 100 m spatial resolution (Santoro et al., 2021). AGB was estimated from living stem volume using wood density and spatialized BEF estimates, where the latter was calculated as a function of branch and leaf biomass to stem (Santoro et al., 2021).

Global Forest Watch (GFW)

This global AGB dataset was obtained from the Global Forest Watch website (https://data.globalforestwatch.org). This dataset has a spatial resolution of 30 m and represents AGB (Mg/ha) for 2000. Standard errors were not available for this dataset. GFW AGB density was estimated using LIDAR and regional allometric equations across more than 700,000 locations globally (Harris et al., 2021). Site-level tree height-biomass equations were linked with satellite or airborne lidar observations to estimate AGB density at these ground-measured biomass plots (Harris et al., 2021). To create a continuous AGB map, random forest models were trained using predictor variables, such as NDVI, tree cover, and monthly mean precipitation (Harris et al., 2021).

European Space Agency (ESA)

This AGB dataset was developed by the ESA Biomass Climate Initiative and was obtained from the Center for Environmental Data Analysis website (version 3) (https://climate.esa.int/en/odp/#/project). The data product has a spatial resolution of 100 m and provides AGB (Mg/ha) and standard error (Mg/ha) estimates for the years 2010 (ESA 2010), 2017 (ESA 2017), and 2018 (ESA 2018) (Santoro and Cartus, 2021). SAR C-band from Envisat ASAR for 2010 and Sentinel -1 for 2017-2018 and L-bands from ALOS-1 POLSAR-1 for 2010 and ALOS-2 POLSAR-2 for 2017-2018data were used to produce the AGB map (Santoro and Cartus, 2021). As the C and L bands have different spatial resolutions, the C-band data were resampled from 150 m to 100 m to match the resolution of the L-band data (Santoro and Cartus, 2021). Then, the two AGB maps obtained from the L and C bands were merged using a set of weighting rules to obtain the final AGB map (Santoro and Cartus, 2021). The algorithm to produce the ESA biomass follows the GB datasets mentioned above.

GEDI

The GEDI L4 gridded AGB density (Mg/ha) and standard error (Mg/ha) data product were obtained from the ORNL DAAC website (https://daac.ornl.gov/). This data product provides AGB estimates at 1 km spatial resolution and is based on GEDI observations acquired for 2019-2021 (Dubayeh et al., 2022). AGB was first estimated for every GEDI footprint with valid height metrics using a parametric model derived from a global set of calibration data. The mean AGB was predicted using a hybrid model-based estimator (Dubayeh et al., 2022). Linear models were applied to each plant functional type and world region to generate the gridded AGB estimates,

which are the results of the application of a hybrid estimator to LIDAR returns within each 1 km grid cell across the tropical and temperate terrestrial ecosystems (Dubayeh et al., 2022).

2.2 TRENDY Models

Besides satellite-derived datasets, we also used AGB simulated by nine dynamic global vegetation models (DGVMs) from the TRENDY Experiment (v10). To eliminate any discrepancies that could arise among models due to different environmental drivers, standardized forcing data such as climate, land cover, and atmospheric CO_2 concentration were used to drive these models. Model simulations are for the period spanning 1700–2020 using standard spin-up and simulation protocols (Sitch et al, 2015). The models are run in an offline simulation using the forcing data provided. Each simulation protocol is designed to test the sensitivity of one of the above-mentioned forcing data. We used the S3 simulation, where all forcing is time-varying. We only use the models that output AGB, GPP, NPP, and autotrophic respiration (Table S1). DGVMs estimate AGB as a function of NPP and carbon allocation factors [El Masri et al., 2013]. In the models, NPP, the difference between GPP and autotrophic respiration, is allocated to the vegetation pools (e.g. stem, leaf, and roots) to build the biomass based on the allocation factors. Also, the carbon allocation to the vegetation pools is constrained by environmental drivers, such as light, nitrogen, and water [El Masri et al., 2013].

2.3. Plant functional type data

To estimate the AGB based on plant functional type (PFT), we used ESA PFT datasets developed for DGVMs (Harper el al., 2023). The dataset consists of 14 PFTs with a 300 m spatial resolution for 1992-2020 produced by combining ESA 300 m land cover data with other land cover datasets (Harper et al., 2023). We extracted 8 woody PFTs: broadleaf deciduous, broadleaf evergreen, needleleaf deciduous, needleleaf evergreen, shrub broadleaf deciduous, shrub broadleaf evergreen, shrub needleleaf deciduous, and shrub needleleaf evergreen. The shrub PFTs were combined into one group for this analysis. We resampled the dataset to 1 km and 1° spatial resolution using the majority method to match the satellite-based and TRENDY AGB resolution, respectively. Then, we extracted the AGB for each PFT and estimated the total AGB as the sum of all the grid cells for each PFT.

2.4 FAO data

We used the AGB data from the FAO Global Forest Resources Assessment Main Report 2020 (https://www.fao.org/forest-resources-assessment/2020/en/). We extracted the regional forest area and total living biomass for 2000, 2010, and 2020. The total FAO mean AGB was calculated and used to assess the total satellite-based AGB and TRENDY model AGB estimates. In other words, we used the FAO total AGB to assess the performance or accuracy of the satellite-based and TRENDY estimated AGB.

2.4 Data Analysis

We calculated the total global AGB for each satellite-derived AGB dataset and quantified the variability of AGB among these products. We calculated AGB for five PFT for each of the five AGB products. To achieve this, we masked the area from the PFT map corresponding to no data or zero value in the AGB datasets. This ensures that the total AGB biomass in Pg is calculated by counting only the grid cells with valid AGB values in a given PFT. Then, the total mean AGB per PFT was calculated by multiplying the total AGB by the total grid area (we converted the area from square meters to hectares) for each of the satellite-derived AGB datasets. Also, we calculated global difference maps in AGB between 2018 and 2010 for the ESA dataset to quantify changes in AGB. In addition, AGB data are in units of dry matter (Mg/ha) and were converted to biomass carbon density (MgC/ha) using a scale factor of 0.5.

The satellite-based AGB datasets reported gridded AGB density and few datasets provided the total AGB per grid cell. We did not use gridded total AGB data due to differences in the forest area used to generate these datasets. Instead, we used the 2010 ESA forest area to estimate the PFT AGB for the satellite-based AGB datasets. By this, we removed the variability between the datasets due to forest area estimates, and the PFT AGB results represent the differences in the methods used to generate the satellite-based AGB datasets.

The satellite-based AGB datasets have spatial resolutions ranging from 30 m to 1 km. We projected all the datasets to equal Earth projection (an equal area projection) to resample the datasets to a common spatial resolution. Using the average resampling method, we resampled these datasets to 1km x 1 km spatial resolution. For each 1 km pixel, its value ws calculated as the average AGB of all the contributing finer-resolution pixels.

The TRENDY model simulations used have a spatial resolution ranging from 0.5° to 1° (Table S1). We resampled the datasets to 1° x 1° spatial resolution so that all the datasets have the same

spatial resolution using the average resampling method after being reprojected to the equal Earth projection. We extracted and calculated the mean AGB, GPP, NPP, and autotrophic respiration for 2000-2020. This is done so that the TRENDY data will represent the same period that the satellite-based AGB was estimated for.

To calculate the latitudinal values, we resampled all the satellite-based AGB data to 1^{o}spatial resolution using the average resampling method. Then, the latitudinal AGB for both the satellite-based AGB and TRENDY-modeled AGB was calculated by extracting the AGB value for each corresponding latitude and averaging the AGB values. All the analyses were conducted using R statistical software and ArcGIS Pro.

3 Results

3.1 Comparison of satellite-derived AGB datasets

Total global AGB ranged from 258 PgC to 385 PgC among the five satellite-based AGB datasets (Fig. 1). The GFW had the highest AGB, followed by ESA 2017. These two datasets had much higher AGB than the other datasets . In addition, the ESA 2010, ESA 2018, GB, and HABdatasets had very similar total AGB. The ESA data showed a decrease of about 16% in AGB between 2017 and 2018 and about 6% decrease in AGB between 2010 and 2018 (Fig. 1). We highlight the spatial variability between the satellite-based AGB datasets rather than comparing their total AGB estimates because the datasets were generated for different years and the AGB will annually vary based on natural (e.g. wildfire) and anthropogenic (deforestation) factors.

We also compared total AGB among the different satellite-derived datasets with the FAO AGB (Fig. 1). Almost all the satellite-derived AGB showed an error of ±4% compared to the FAO mean AGB estimates. GFW overestimated the FAO mean by 27% and GEDI underestimated the FAO mean AGB by 15%. We note that GEDI collects data above the tropical and temperate regions and is expected to underestimate the global AGB estimates. The meansatellite-derived AGB estimate was 316 PgC similar to the FAO mean AGB for the years 2000-2020 of 303 PgC (Fig. 1). To examine the effect of the land cover area on AGB estimates, we used the FAO total forest (FAO, 2020) area to recalculate the total AGB for each of the satellite datasets by multiplying the global average AGB (Mg/ha) by the FAO total forested area (ha). Then, we compared the satellite-based AGB against FAO's estimated average AGB for 2000, 2010, and

2020. The results showed that satellite-based AGB products underestimated the FAO total AGB by more than 50% (Fig S1). . We demonstrate the impacts of forest area on AGB by calculating the forest area based on the ESA PFT forest area by multiplying the grid area by the corresponding percentage of forest cover to estimate the the global total AGB.

Spatially, the ESA data showed higher AGB in Eurasia, North America, and particularly in the tropics than the other AGB datasets (Fig. 3). The HAB data showed the lowest AGB density (~150 MgC/ha) in the topics, while the other datasets showed values up to 300 MgC/ha (Fig. 3). We note here that GEDI data are collected between latitudes of 51^{o} N and S because of the International Space Station's orbit (Dubayah et al., 2022) and thus does not include AGB data for most of the boreal forest.

The standard error for all the AGB data used was higher in tropical areas (Fig. 4). In general, the higher the estimated AGB, the higher the standard error. It is interesting to note that the standard error was lower in the ESA 2017 data compared to the ESA 2010 or 2018 data. The spatial distribution and magnitude of the ESA 2017 standard errors were different from those of the ESA 2010 or 2018 (Fig. 4). GEDI showed the lowest standard errors with values mostly below 40 MgC/ha (Fig. 4).

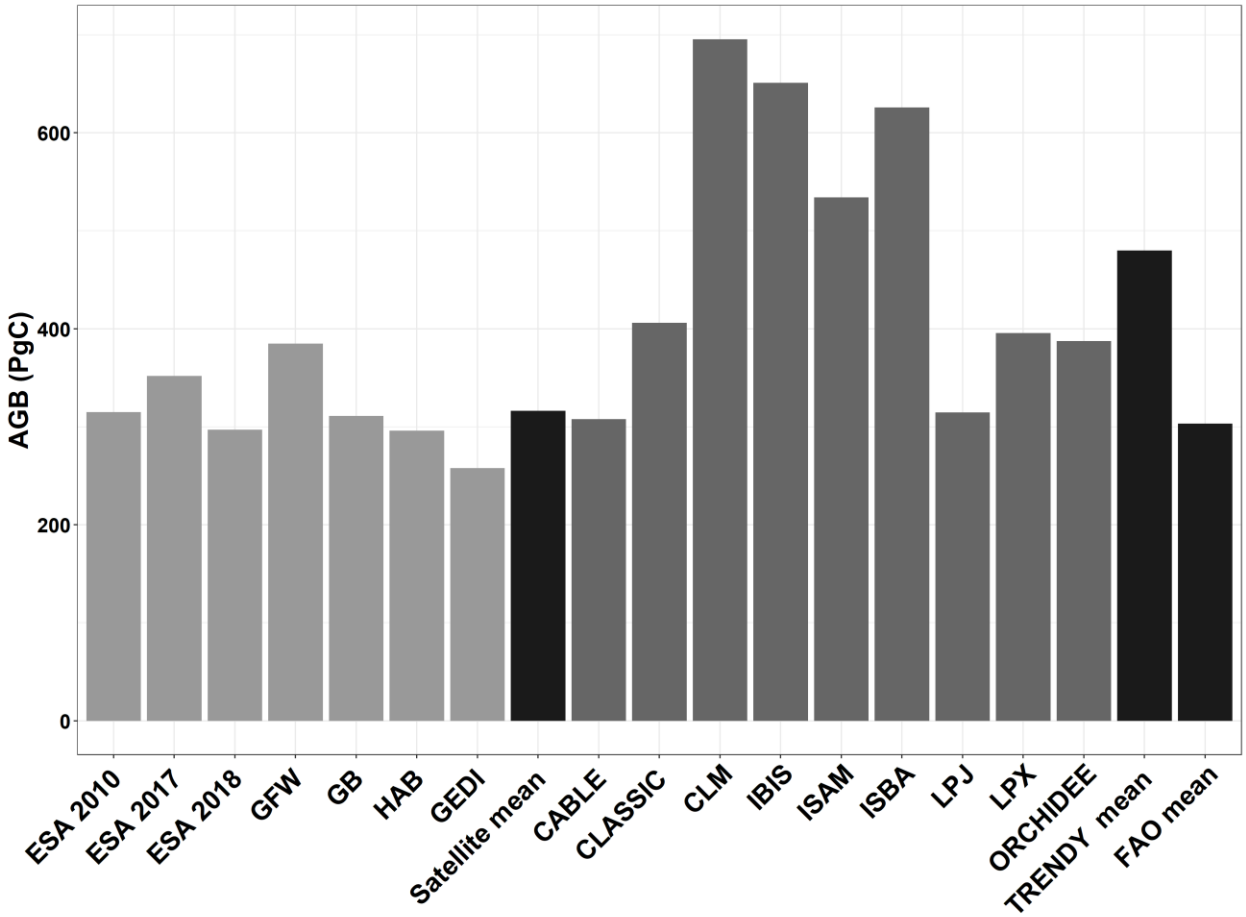

Figure 1. Comparison of total AGB (PgC) estimates among the satellite-derived AGB datasets (light gray bars) and the TRENDY model simulations (dark gray bars) . The two black bars represent the mean of the satellite-derived and TRENDYmodels data, respectively.

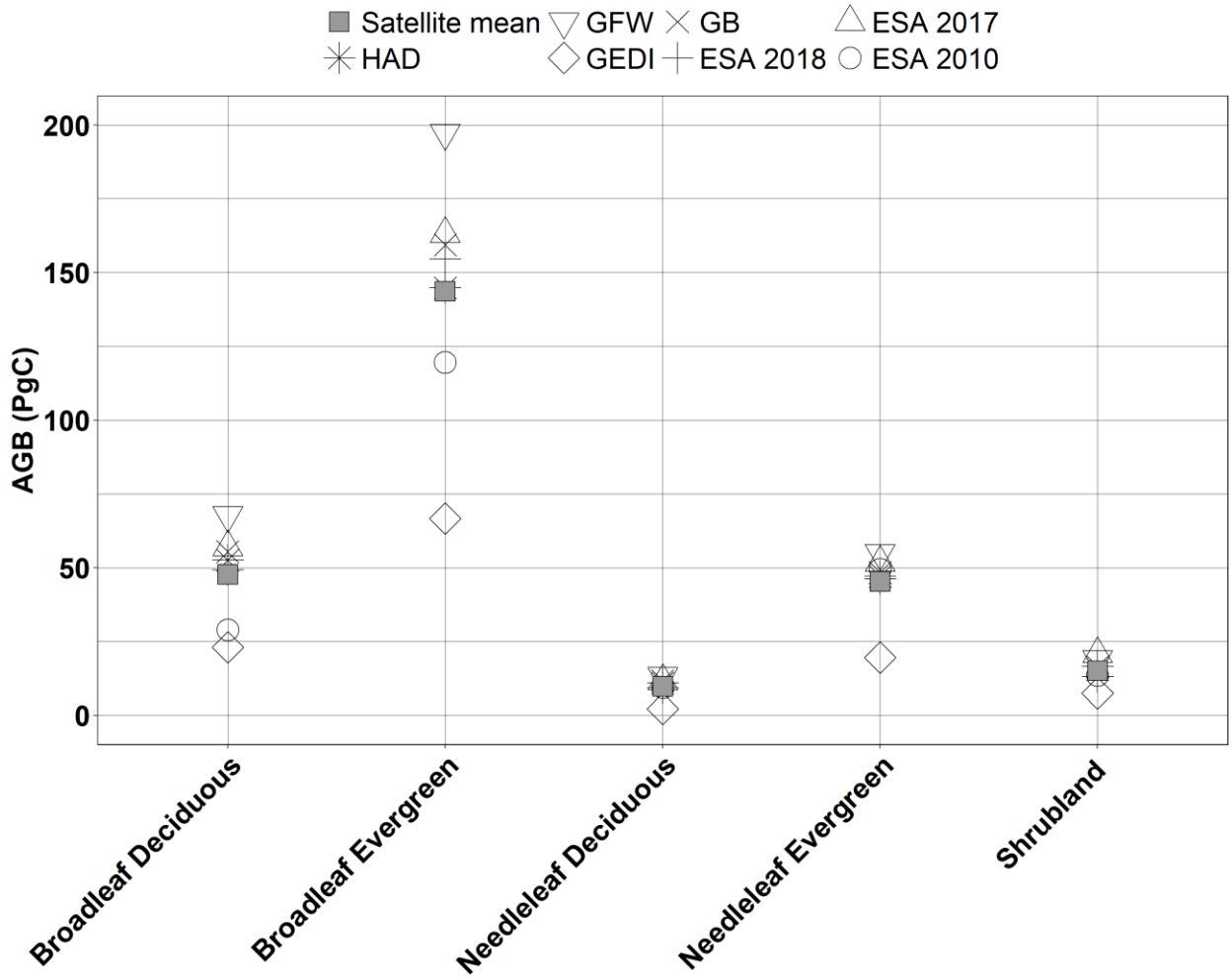

Figure 2Plant fucntional type (PFT) total AGB (PgC) based on the satellite-derived AGB datasets.. We used the ESA PFT area for 2000 to calculate the total AGB for the GFW; the 2010 ESA PFT area was used to calculate the total AGB for ESA 2010, 2017, and 2018, GB, and HAD data; and the 2020 ESA PFT area was used to calculate total AGB for the GEDI data.

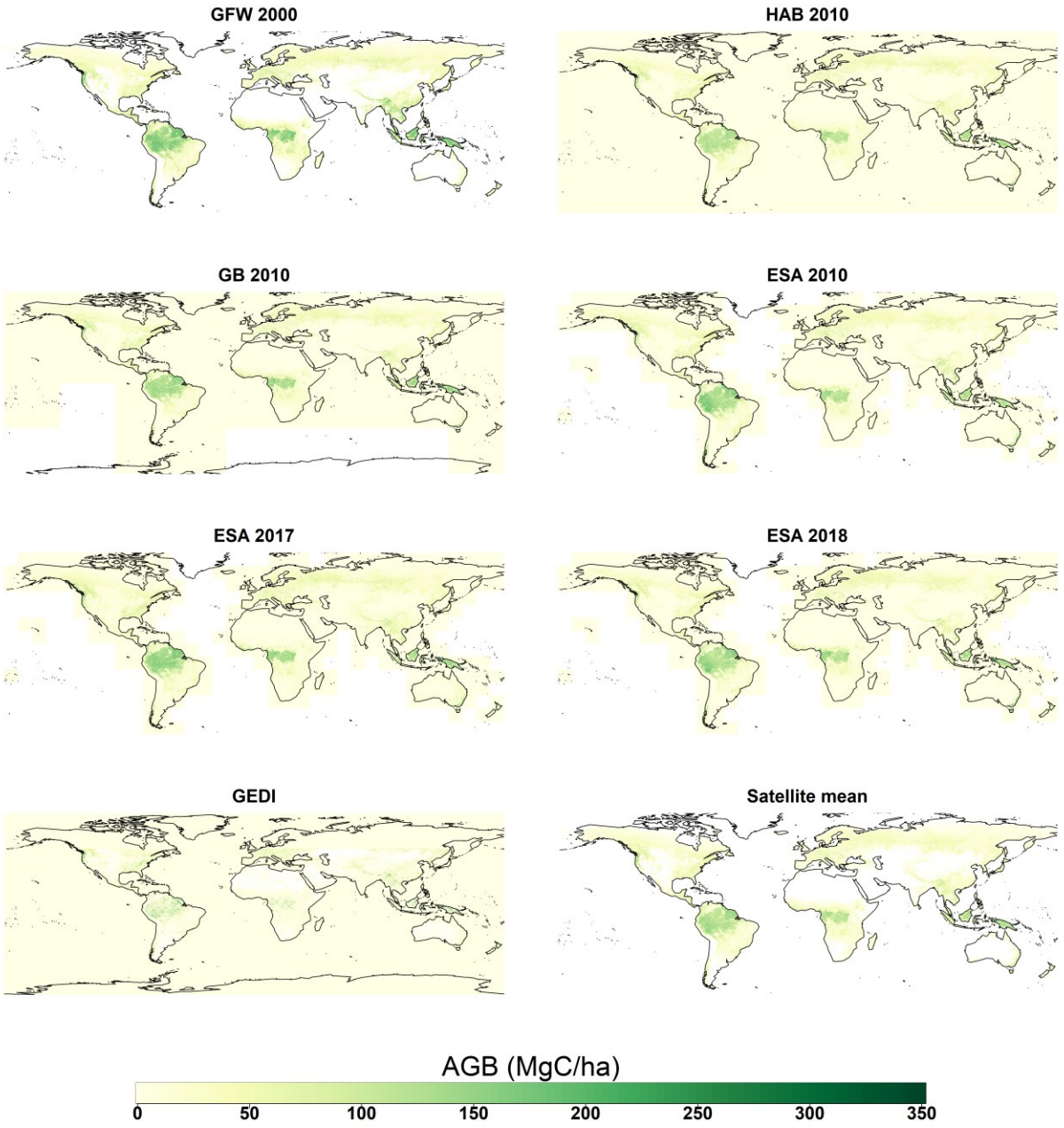

Figure 3. Spatial variability in AGB density among the different satellite-derived AGB datasets. The satellite mean was calculated as the average of the five satellite-bsed AGB datasets.

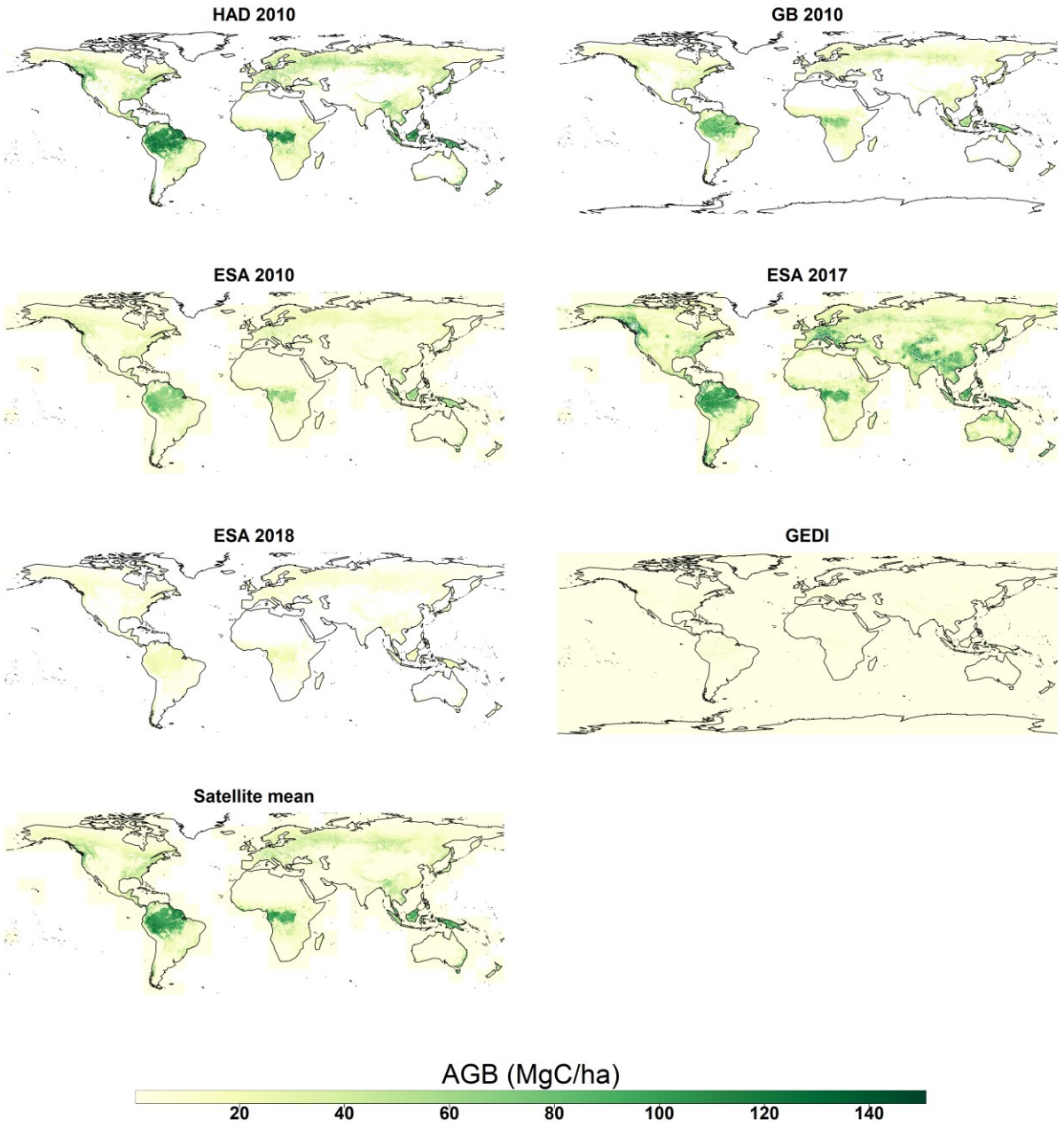

295

296 Figure 4. Spatial variability in AGB standard errors as reported by each of the satellite-derived
297 AGB datasets. The standard errors for the GFW AGB dataset were not provided and therefore
298 were not plotted.

Figure 5 shows the latitudinal viability in AGB density for each of the different satellite-based AGB datasets. Generally, AGB density showed a peak between -15^{o} N and S as well as a smaller peak around -40^{o} S (Fig. 5A). These peaks corresponded to the tropical forest zone and the temperate forest in the southern hemisphere (e.g. southern Australia, New Zealand, Chile, and Argentina). The AGB decreased from the topical latitudes to the temperate and boreal latitudes (Fig. 5A). The GFW showed a peak between 15^{o} and 30^{o} N in the northern subtropical area (Fig. 5A). Furthermore, the large differences in latitudinal patterns among the datasets were likely caused by the differences in the algorithms and satellite data used to generate the AGB data. For instance, GB and ESA data had similar algorithms and satellite data and thus showed similar latitudinal variability in AGB density (Fig. 5A).

The pattern in AGB standard errors along the latitude was similar for all the datasets except for ESA 2017 (Fig. 5B). The AGB standard error had the highest values in the tropical latitudes, then decreased in temperate latitudes, and increased again in the boreal latitudes (Fig. 5B). The magnitude of the AGB standard error in ESA 2017 was more than three times higher than that of the other datasets and ESA 2017 showed higher standard error in the southern hemisphere (Fig. 5B). The peak in standard error around latitude 30^{o}N (Fig 5. B) could be due to the increase in the standard errors in Asia (e.g., China and India) in the ESA 2017 (Fig. 4).

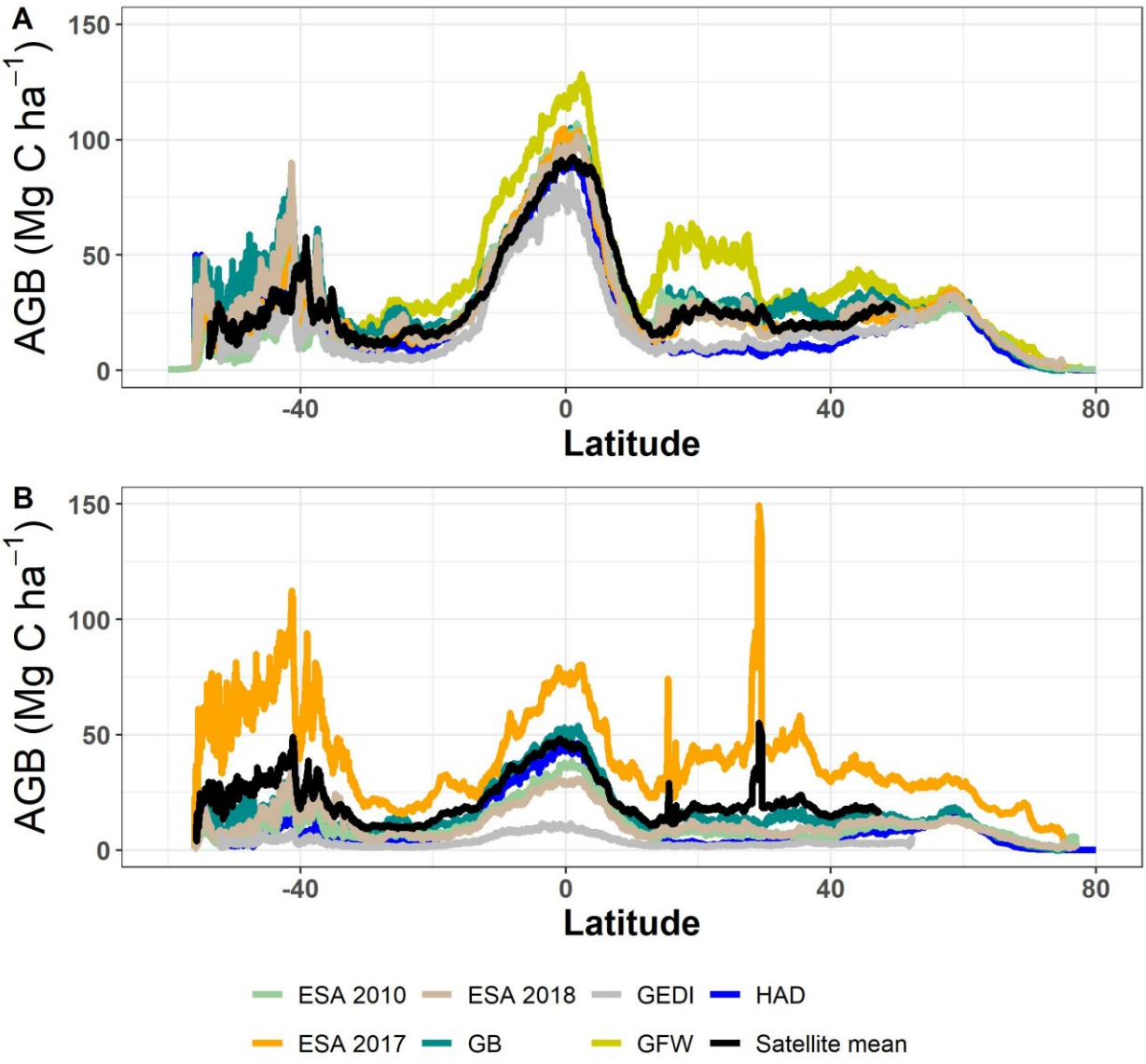

Figure 5. Latitudinal variability in AGB density for each of the satellite-based AGB datasets: (A) AGB; and (B) standard error of AGB density. The standard error is not available for the GFW AGB dataset.

3.2 Evaluation of TRENDY AGB estimates

The total global AGB based on the TRENDY model simulations varied from 307 PgC for CABLE to 696 Pg C for CLM (Fig. 1). The TRENDY mean AGB showed higher AGB density for broadleaf evergreen forest (tropical forest) by about 28% compared to the mean satellite-based AGB estimates and overestimated AGB density by more than 50% in for shrublands (Fig. 2 and Fig. 6). The mean of the TRENDY AGB estimate was close to that of the satellite-based

AGB estimates for almost all the PFTs (Fig. 6) but showed higher global AGB estimates (494PgC) by about 164 PgC when compared to the satellite-based meanAGB estimate(316PgC).

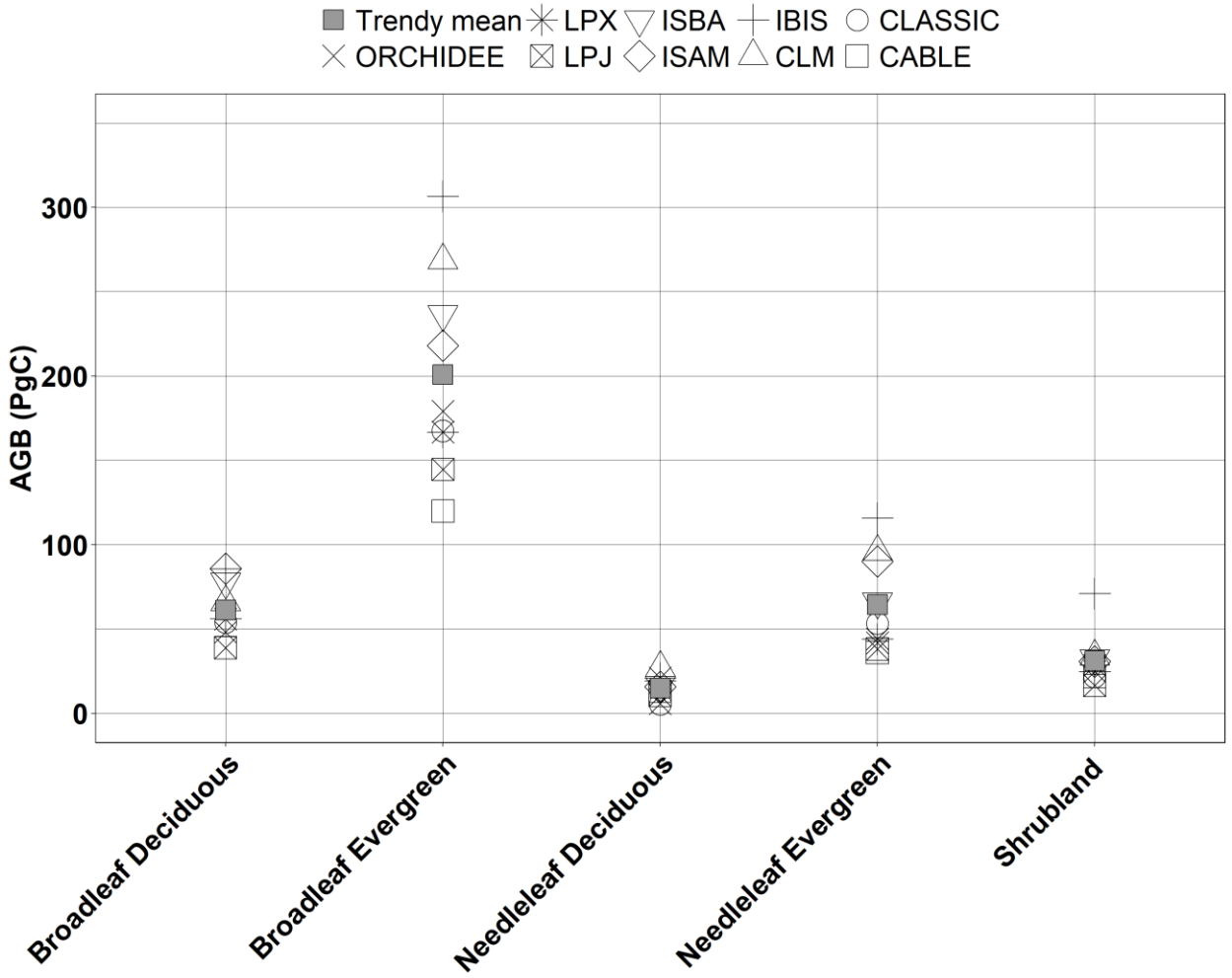

Figure 6. Plant fucntioal type (PFT) total AGB (PgC) based on TRENDY models . The ESA mean PFT area for 2000-2020 was used for the calculation of regional total AGB for TRENDY models.

We also compared the TRENDY AGB estimates with the FAO average AGB for the years 2000, 2010, and 2020 to match the TRENDY AGB period used in this study. In general, TRENDY-based AGB estimates overestimated AGB for the years 2000-2020 (Fig. 1). The TRENDY ensemble mean overestimated the FAO mean AGB by about 37%, whereas the satellite-based AGB ensemble mean underestimated the FAO mean AGB by 4% (Fig. 6). We note here that the use of different forest areas resulted in a significant change in regional and total AGB,

highlighting the need for a comprehensive forest area dataset to reduce errors in global AGB estimates.

All TRENDY models showed the highest AGB density around the tropical areas and few models (CLM5.0, ISAM, and IBIS) also showed high AGB in the northern mid-latitude areas (Fig. 7). Although the spatial pattern of AGB density looked similar among the TRENDY models, the magnitude of AGB varied substantially among the models. For instance, CLM5.0 AGB reached 350 Mg/ha in tropical areas, which is almost twice the AGB values for the CABLE model (Fig. 7). In general, the TREDNY and the satellite-based AGB products showed similar spatial patterns.

Figure 8 shows the latitudinal pattern of AGB density for each of the TRENDY models. Generally, AGB density showed the highest peak between 15^{o} N and 15^{o} S as well as a smaller peak around 40^{o} S and 60^{o} N (Fig. 8). These peaks corresponded to the tropical forest zone and the temperate forest in the southern and northern hemispheres as well as the high latitude areas in the northern hemispheres, which was similar to the latitudinal pattern of the satellite-based AGB density (Fig. 5A). Large variability in latitudinal pattern existed among the models with the highest variability around the tropical areas, where IBIS estimated AGB was more than three times higher than that of CABLE (Fig. 8). Similarly, satellite-derived AGB data showed great variability and similar divergence to the TRENDY models (Fig. 5A). The high variability in the latitudinal pattern of AGB density among the TRENDY models is due to the differences in the algorithms and schemes used to estimate the AGB data. For instance, models with low autotrophic respiration (R_a) and gross primary production (GPP), such as the LPX model, had higher NPP and thereby higher AGB than the CABLE model that had higher R_a but similar GPP to the LPX model (Fig. S5).

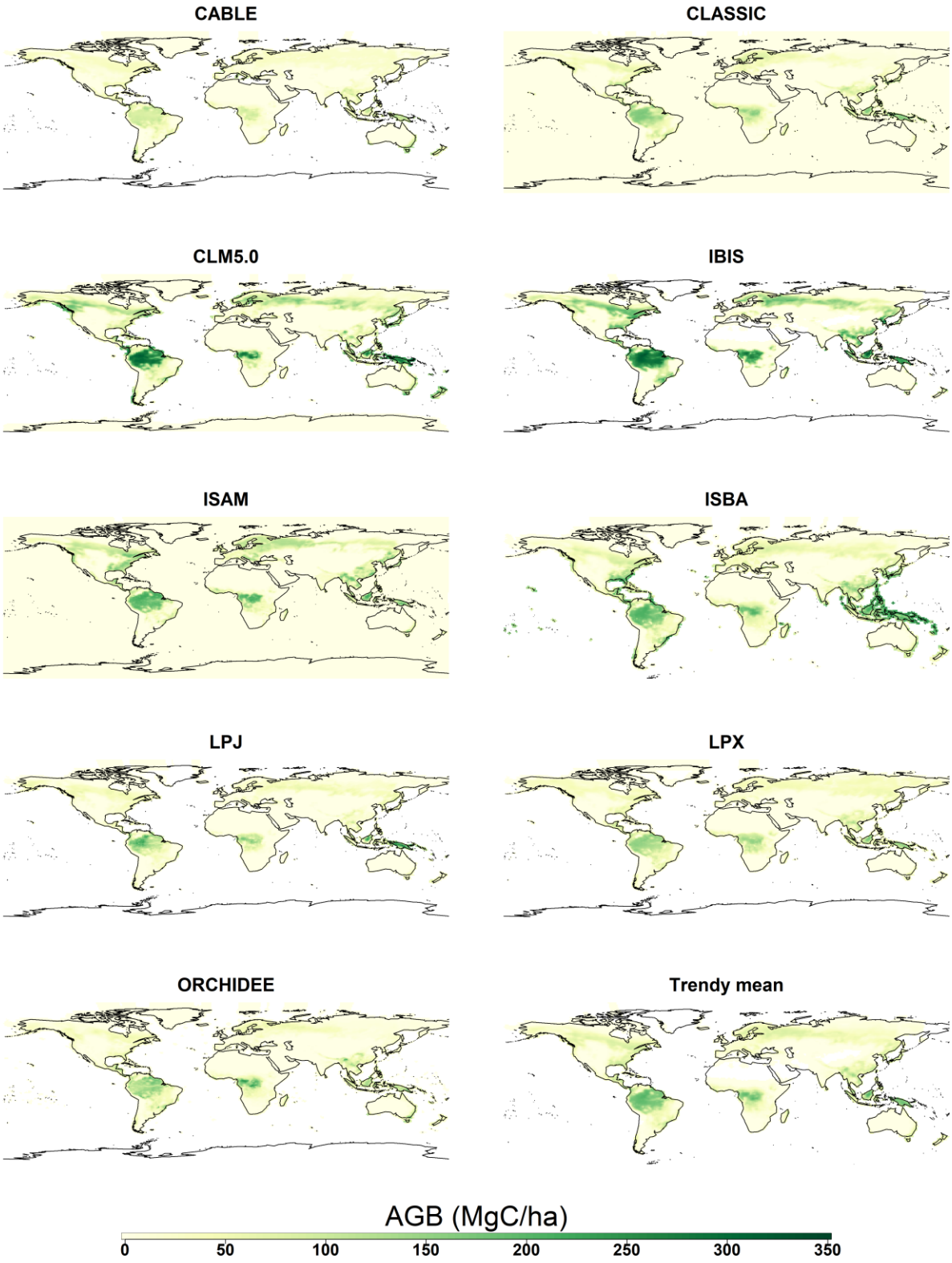
CABLE
CLASSIC
CLM5.0
IBIS
ISAM
ISBA
LPJ
LPX
ORCHIDEE
Trendy mean
AGB (MgC/ha)
0
50
100
150
200
250
300
350

363

364 Figure 7. Spatial variability in the mean AGB density over the period 2000-2020 for the
365 TRENDY models. All the data were resampled to 0.5° resolution using the nearest neighbor
366 method.

367

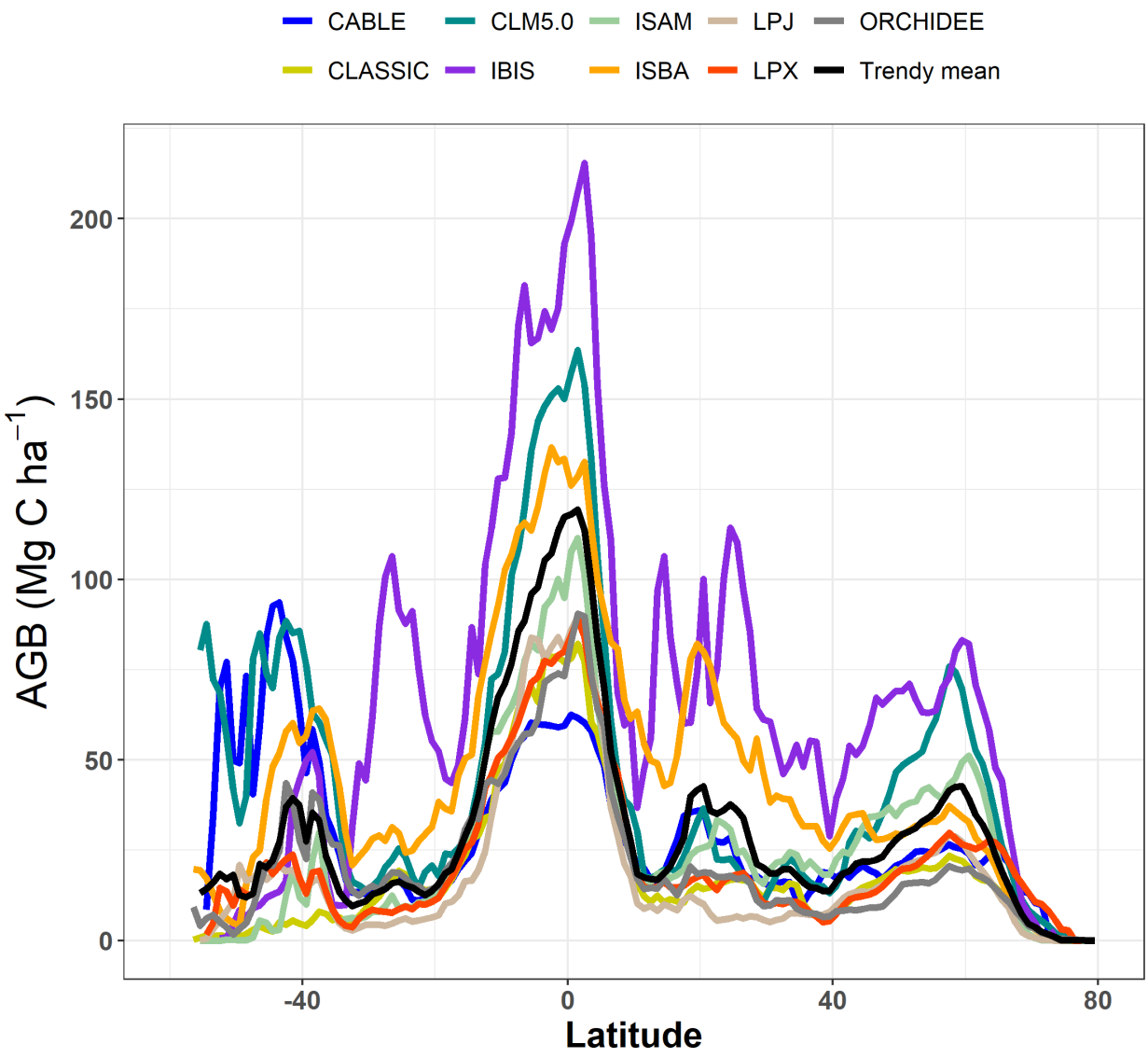

368

369 Figure 8. The latitudinal pattern of mean AGB density over the period 2000-2020 for each of the
370 TRENDY models and the ensemble mean.

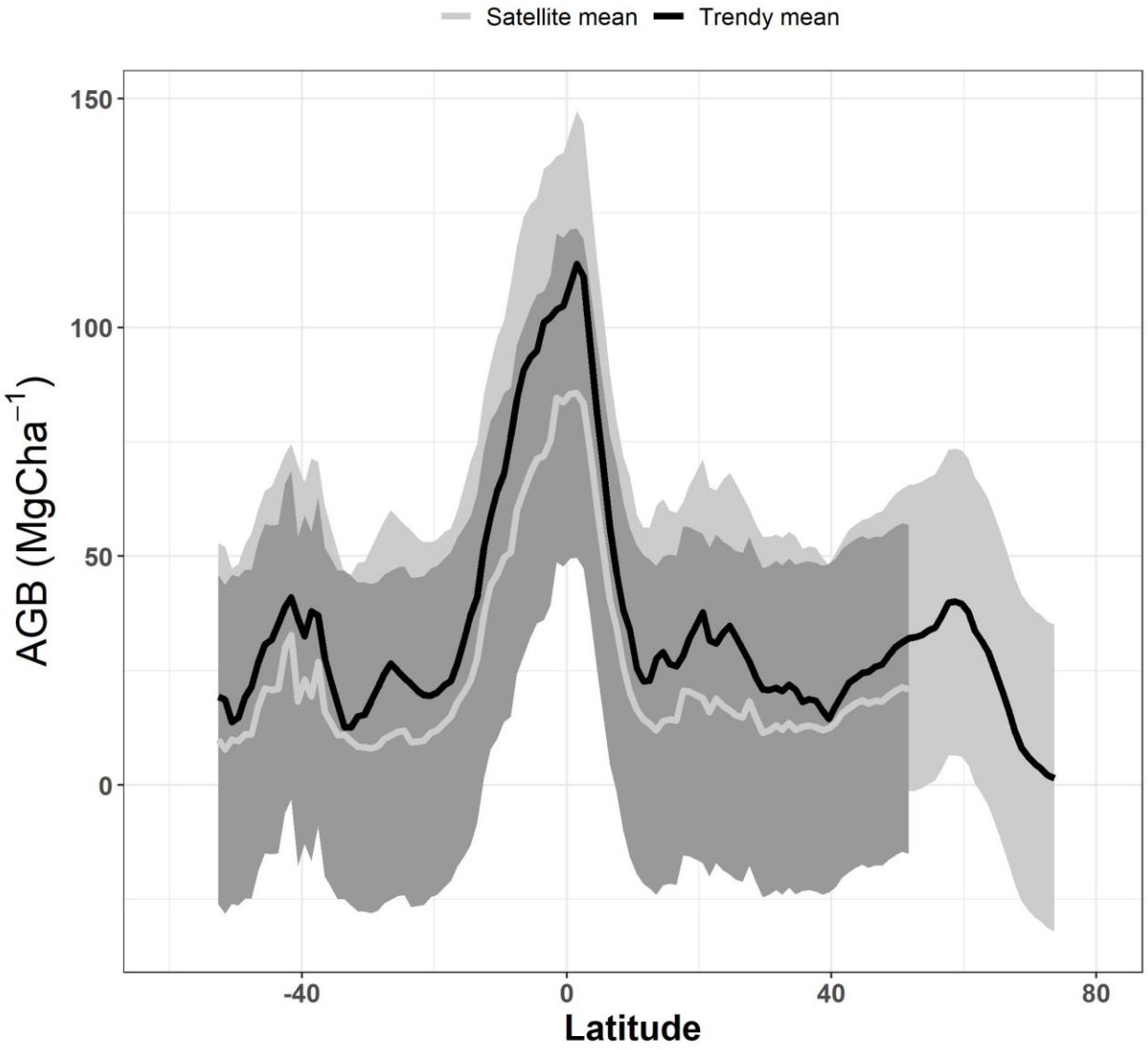

Figure 9. The latitudinal pattern in TRENDY ensemble mean (gray line) and satellite-based ensemble mean (black line) AGB density estimates. The shaded area represents the standard deviation in satellite-based AGB estimates (dark gray) and TRENDY model estimates (light gray).

We compared the latitudinal pattern in the TRENDY AGB density mean and the satellite-based AGBmean (Fig. 9). In general, the latitudinal patterns were similar except for the peak in the northern hemisphere mid-latitudes in the TRENDY AGB estimates (Fig. 9). The TRENDY mean shows a drastic increase in AGB density around 20^{o} latitude north and south, which is not in agreement with the mean satellite-based AGB (, which could be due to differences in land cover

and land use between the datasets (Fig. 9). The shaded area in Figure 9 shows that the TRENDY datasets had less spread than the satellite-based datasets. This can be attributed to using the same land cover dataset as required by the TRENDY modeling protocol to minimize the uncertainty that arises from the use of different land cover data.

4. Discussion

4.1. Satellite-based AGB estimates

We find that the satellite-based AGB products disagree in the magnitude of AGB density, which reflects the differences in methods and remote sensing data used. The latitudinal patterns of AGB density showed the highest variability around the tropical areas likely due to dense and complex canopies, saturation of satellite signals, sparse satellite data availability, or insufficient site data to calibrate the predictive models (Xiao et al., 2019; Englhart et al., 2021). Our analysis revealed little change in total AGB between 2010 and 2018, but a significant decrease of about 40% in the total AGB between 2000 and 2018.

When compared to the averaged FAO AGB data, the ESA 2018 and HADB are the most accurate as they had the lowest mean absolute error (6.3 and 7.3 PgC, respectively). We note that no dataset performed well for all the PFTs and our recommendation is based on the global total mean absolute error. This does not indicate that the other AGB datasets are not reliable and we recommend that users perform a bias analysis to determine which product performs the best for their study area or region.

The differences that we found among the satellite-based AGB estimates can be traced back to the input data and algorithms used to generate the AGB estimates. The ESA AGB estimates showed a slight increase in 2017 and an almost 10% decrease in 2018. This can be attributed to the different remote-sensing sensors used and algorithm improvements to generate these datasets (Santoro et al., 2021; Santoro and Cartus, 2018, 2021). Moreover, GEDI AGB was retrieved from GEDI LIDAR data and averaged to a grid cell using a hybrid model estimator (Dubayeh et al., 2022) resulting in a different spatial distribution and magnitude of AGB. Nevertheless, algorithm modifications and the use of LIDAR data are recommended to improve satellite-based AGB estimates.

The satellite-based AGB standard errors were about 25% of the total AGB values, particularly for the tropical areas. This can be related to the remote sensing data inputs used to generate these products. Several challenges such as saturation of optical remote sensing data in dense and

complex canopies and frequent cloud cover can limit the ability of optical remote sensing to acquire data in tropical areas (Flores-Anderson, et al., 2023, Zhao et al., 2016). LIDAR and RADAR data are not affected by cloud cover with high penetration capacity allowing for the retrieval of the vertical distribution of organic matter, such as tree height, for improving AGB estimation (Santoro and Cartus, 2018; Su et al., 2020). However, many studies have demonstrated the limitation of RADAR and LIDAR data in estimating AGB, including RADAR signal saturation at high AGB (Joshi et al., 2017; Woodhouse et al., 2012), and the temporal and spatial coverage of spaceborne LIDAR with low-density footprint limiting its applications in global AGB estimation (Hu et al., 2016). However, finer spatial and temporal resolutions of LIDAR remote sensing decreased the standard errors as observed using GEDI AGB data. It is expected that with the availability of new LIDAR and RADAR (e.g. soon-to-be-launched Biomass Monitoring Mission for Carbon Assessment (Biomass) and the NASA ISRO Synthetic Aperture Radar (NISAR)) data, errors in modeling AGB in the tropical area will be further reduced.

The differences in the variability of latitudinal patterns in AGB density among the satellite-based AGB datasets can be related to the forested area used to generate these products. For instance, the forested area in South America used to estimate AGB is 1990 Million ha and 2251 Million ha for HAD and GB datasets, respectively (Harris et al 2021; Santoro et al., 2021), resulting in significant differences in the estimated AGB. Whereas, datasets that used ESA land cover data (e.g. GB, ESA) have similar latitudinal patterns in AGB density although the AGB magnitude was different. We note that the spread in AGB among the satellite-based AGB products can be related to the different satellite data used to generate the datasets. Nevertheless, accurate representation or mapping of forested areas is key to improving future satellite-based AGB estimates.

Future satellite-based products need to harness the increased availability of satellite imagery with different spatial and temporal scales and to explore how such diverse data impact the accuracy of the satellite-based AGB estimates. For instance, satellite-based AGB estimation accuracy was improved by fusing Sentinel-2 and ICESAT-2 data (Jiang et al., 2022) and Landsat 8 with Sentinel-1A (Li et al., 2020). Vegetation optical depth (VOD) derived from passive microwave remote sensing data has proven effective in quantifying AGB at regional to global scales (Yu et al., 2024). The fusion of passive remote sensing data (e.g., VOD) with newly available active

remote sensing data (e.g., tree height) might help in decreasing the uncertainty in satellite-based AGB estimates. Moreover, the use of machine learning methods has shown the potential to improve the accuracy of the AGB estimates (Jiang et al., 2022; Li et al., 2020). A new comprehensive analysis of ensemble machine learning methods with different configurations for improving AGB estimates is needed. Given that, more field data is required to calibrate and validate these approaches to decrease and quantify the uncertainty in satellite-based AGB estimates.

4.2. TRENDY Models

We find that the AGB simulated by the TRENDY models disagreed in the magnitude of AGB due to the differences in model structure and parameterization. These models differ in the representation of ecosystem processes (e.g., photosynthesis, carbon allocation, respiration) and the interactions among climate, atmospheric CO_2 concentration, and N-deposition (Sitch et al., 2015; Yang et al., 2020). Interestingly, whether a model considers C-N coupling does not appear to influence AGB since the C-only models (ISBA and CLASSIC) showed similar values to the C-N models (Fig. 8), but showed the highest values for GPP and R_a (Figs. S3 and S5). This can be attributed to model parametrization and carbon allocation rates influencing carbon storage in the woody structure (El Masri et al., 2013).

The global total AGB predicted by the TRENDY models was higher than that of the satellite-based AGB estimates (Figure 1). The differences in the total AGB between the TRENDY models and satellite-based AGB datasets could be due to the different assumptions related to wood turnover rates and autotropic respiration (R_a) schemes used in the models. The latitudinal pattern in R_a is highly variable among the models (Fig. S5) explaining some differences between the TRENDY models' AGB estimates and the satellite-based AGB datasets. Despite that, the AGB spatial distribution is similar between the TRENDY models and the satellite-based AGB estimates. This indicates that the TRENDY models' processes can capture the spatial variability in AGB density, but not the magnitude well. For instance, TRENDY models underestimated the satellite-based AGB density in the northern hemisphere and this can be attributed in part to autotrophic respiration drivers, such as the carbon allocation scheme, that vary between the models (El Masri et al., 2019). In addition, the discrepancy between the models' estimated AGB and the satellite-based AGB estimates for the tropical zone (Figs.3 & 7) can be due to processes that lead to a decrease in biomass such as high wood turnover rates or high autotrophic

respiration rates. Nevertheless, the the satellite-based mean AGB is comparable to the FAO total AGB, indicating that satellite-based mean AGB can be used to benchmark AGB simulated by DGVMs. Future work should focus on improving the satellite-based and models' total AGB estimates as well as improving the AGB spatial variability to reduce the uncertainty in the AGB estimates.

We find that the latitudinal variability in the means AGB density is similar between the TRENDY models and the satellite-based datasets (Fig.9). The TRENDY model mean overestimated AGB in the mid-latitudes (30N and 30S) compared to the satellite-based mean. This is likely due to the high AGB values in the IBIS mode estimates (See Figure 5). The differences in the forested area used in the TRENDY model and the satellite-based AGB estimates might explain the underestimation of AGB by the TRENDY models between latitudes 30N and 50N (Fig. 9). For instance, a decrease in the forested area will lead to a decrease in AGB which can be related to a decrease in GPP and NPP for the TRENDY models (See Figures S3-S4).. The carbon allocation factors and/or autotrophic respiration rates for vegetation pools are likely the main drivers for this peak. Further experimentation is needed to modify model processes (e.g. carbon allocation, carbon turnover rates, and autotrophic respiration) that lead to observed differences in the latitudinal patterns in TRENDY model estimated AGB and satellite-based AGB estimates.

5 Conclusions

Detailed analysis of satellite-based AGB estimates and DGVM AGB simulations provides necessary information about algorithms, input data, and the assumptions used. On average, we find that satellite-based AGB products and modeled AGB agree on the global spatial distribution of AGB density, with the highest density in the tropical regions. The uncertainties and errors in satellite-based AGB can be mostly attributed to uncertainties in the forest cover and availability of remote sensing data in regions with dense and complex canopies and persistent cloud cover (e.g., tropics). The TRENDY models' AGB estimates can be improved through a comparison with the mean of satellite-based AGB estimates. Such a practice can help constrain the AGB values and hopefully lower the standard errors in the AGB estimates of the DGVMs. Future satellite-based AGB datasets should take advantage of the increased availability of LIDAR data as well as the use of machine learning methods to reduce errors and improve the AGB estimates. Key missing information can be identified by synthesis of existing in situ data (e.g. plot-level

AGB and tree height) to constrain the estimates and reduce the errors. The use of different forest area maps can lead to discrepancies in AGB among the different satellite-based AGB datasets. We call on new intercomparison studies not only to focus on AGB drivers (e.g., LAI, NDVI, etc.) and algorithms but also on forested area data.

Acknowledgments

- B. El Masri was supported by NASA Kentucky under NASA award No: 80NSSC20M0047, NASA Kentucky R3 award, DOE (Environmental System Science: DE-SC0022228), and NSF (NSF EPSCoR Fellowship: 2327374). J. Xiao was supported by NASA (GEDI Science Team: 80NSSC24K0601) and NSF (Macrosystem Biology and NEON-Enabled Science program: DEB-2017870). We acknowledge the Global Carbon Project, which is responsible for the Global Carbon Budget and we thank the land modeling groups for producing and making available their model output and the two anonymous reviewers for their constructive comments on our manuscript.

Data availability

The TRENDY and satellite datasets are available publicly through the website of each dataset. TRENDY data was obtained from the Global Carbon Budget data website (TRENDY, 2021). The ESA global plant functional type dataset v2.0.8 (Harper et al., 2023) is obtained from the the ESA CEDA Archive website.The harmonized aboveground and belowground carbon density (MgC/ha) for the year 2010 is available from the Oak Ridge National Lab Distributed Archive Center for Biogeochemical Dynamics (ORNL DAAC) website (Spawn et al., 2020). The global aboveground biomass data are available from the Global Biomass website (Santoro et al., 2018). The global aboveground biomass data are available from the Global Forest Watch website (GFW, 2022). The ESA Biomass Climate Initiative global data are available from the Center for Environmental Data Analysis website (version 3) (Santoro and Cartus, 2021). The GEDI L4 gridded AGB density data are available from the ORNL DAAC website (Dubayah et al., 2023)

References

Ahlström, A., Schurgers, G., & Smith, B. (2017). The large influence of climate model bias on terrestrial carbon cycle simulations. *Environmental Research Letters*, *12*(1), 014004. https://doi.org/10.1088/1748-9326/12/1/014004

Anderson, J. E., Plourde, L. C., Martin, M. E., Braswell, B. H., Smith, M.-L., Dubayah, R. O., Hofton, M. A., & Blair, J. B. (2008). Integrating waveform lidar with hyperspectral imagery for inventory of a northern temperate forest. *Remote Sensing of Environment*, *112*(4), 1856–1870. https://doi.org/10.1016/j.rse.2007.09.009

Araza, A., de Bruin, S., Herold, M., Quegan, S., Labriere, N., Rodriguez-Veiga, P., Avitabile, V., Santoro, M., Mitchard, E. T. A., Ryan, C. M., Phillips, O. L., Willcock, S., Verbeeck, H., Carreiras, J., Hein, L., Schelhaas, M.-J., Pacheco-Pascagaza, A. M., da Conceição Bispo, P., Laurin, G. V., … Lucas, R. (2022). A comprehensive framework for assessing the accuracy and uncertainty of global above-ground biomass maps. *Remote Sensing of Environment*, *272*, 112917. https://doi.org/10.1016/j.rse.2022.112917

Blaško, R., Forsmark, B., Gundale, M. J., Lim, H., Lundmark, T., & Nordin, A. (2022). The carbon sequestration response of aboveground biomass and soils to nutrient enrichment in boreal forests depends on baseline site productivity. *Science of The Total Environment*, *838*, 156327. https://doi.org/10.1016/j.scitotenv.2022.156327

DeFries, R. S., Houghton, R. A., Hansen, M. C., Field, C. B., Skole, D., & Townshend, J. (2002). Carbon emissions from tropical deforestation and regrowth based on satellite observations for the 1980s and 1990s. *Proceedings of the National Academy of Sciences*, *99*(22), 14256–14261. https://doi.org/10.1073/pnas.182560099

Dubayah, R., Armston, J., Healey, S. P., Bruening, J. M., Patterson, P. L., Kellner, J. R., Duncanson, L., Saarela, S., Ståhl, G., Yang, Z., Tang, H., Blair, J. B., Fatoyinbo, L., Goetz, S., Hancock, S., Hansen, M., Hofton, M., Hurtt, G., & Luthcke, S. (2022). GEDI launches a new era of biomass inference from space. *Environmental Research Letters*, *17*(9), 095001. https://doi.org/10.1088/1748-9326/ac8694

Dubayah, R., Blair, J. B., Goetz, S., Fatoyinbo, L., Hansen, M., Healey, S., Hofton, M., Hurtt, G., Kellner, J., Luthcke, S., Armston, J., Tang, H., Duncanson, L., Hancock, S., Jantz, P., Marselis, S., Patterson, P. L., Qi, W., & Silva, C. (2020). The Global Ecosystem Dynamics Investigation: High-resolution laser ranging of the Earth's forests and

562 topography. *Science of Remote Sensing*, *1*, 100002.
563 https://doi.org/10.1016/j.srs.2020.100002
564 Dubayah, R.O., J. Armston, S.P. Healey, Z. Yang, P.L. Patterson, S. Saarela, G. Stahl, L.
565 Duncanson, J.R. Kellner, J. Bruening, and A. Pascual. 2023. GEDI L4B Gridded
566 Aboveground Biomass Density, Version 2.1. [Dataset] ORNL DAAC, Oak Ridge,
567 Tennessee, USA. https://doi.org/10.3334/ORNLDAAC/2299
568 El Masri, B., Schwalm, C., Huntzinger, D. N., Mao, J., Shi, X., Peng, C., Fisher, J. B., Jain, A.
569 K., Tian, H., Poulter, B., & Michalak, A. M. (2019). Carbon and Water Use Efficiencies:
570 A Comparative Analysis of Ten Terrestrial Ecosystem Models under Changing Climate.
571 *Scientific Reports*, *9*(1), 14680. https://doi.org/10.1038/s41598-019-50808-7
572 El-Masri, B., Barman, R., Meiyappan, P., Song, Y., Liang, M., & Jain, A. K. (2013). Carbon
573 dynamics in the Amazonian Basin: Integration of eddy covariance and ecophysiological
574 data with a land surface model. *Agricultural and Forest Meteorology*, *182–183*, 156–167.
575 https://doi.org/10.1016/j.agrformet.2013.03.011
576 Englhart, S., Keuck, V., & Siegert, F. (2011). Aboveground biomass retrieval in tropical
577 forests—The potential of combined X- and L-band SAR data use. *Remote Sensing of*
578 *Environment*, *115*(5), 1260–1271. https://doi.org/10.1016/j.rse.2011.01.008
579 FAO. (2020). *Global Forest Resources Assessment 2020: Main report*. FAO. [Dataset]
580 https://doi.org/10.4060/ca9825en
581 Flores-Anderson, A. I., Cardille, J., Azad, K., Cherrington, E., Zhang, Y., & Wilson, S. (2023).
582 Spatial and Temporal Availability of Cloud-free Optical Observations in the Tropics to
583 Monitor Deforestation. *Scientific Data*, *10*(1), 550. https://doi.org/10.1038/s41597-023-
584 02439-x
585 Friedlingstein, P., Jones, M. W., O'Sullivan, M., Andrew, R. M., Bakker, D. C. E., Hauck, J., Le
586 Quéré, C., Peters, G. P., Peters, W., Pongratz, J., Sitch, S., Canadell, J. G., Ciais, P.,
587 Jackson, R. B., Alin, S. R., Anthoni, P., Bates, N. R., Becker, M., Bellouin, N., Zeng, J.
588 (2022). Global Carbon Budget 2021. *Earth System Science Data*, *14*(4), 1917–2005.
589 https://doi.org/10.5194/essd-14-1917-2022
590 Gerber, S., Hedin, L. O., Keel, S. G., Pacala, S. W., & Shevliakova, E. (2013). Land use change
591 and nitrogen feedbacks constrain the trajectory of the land carbon sink. *Geophysical*
592 *Research Letters*, *40*(19), 5218–5222. https://doi.org/10.1002/grl.50957

GFW. (2022). Aboveground Live Woody Biomass Density. [Dataset] https://data.globalforestwatch.org/datasets/gfw::aboveground-live-woody-biomass-density/explore

Hall, F. G., Bergen, K., Blair, J. B., Dubayah, R., Houghton, R., Hurtt, G., Kellndorfer, J., Lefsky, M., Ranson, J., Saatchi, S., Shugart, H. H., & Wickland, D. (2011). Characterizing 3D vegetation structure from space: Mission requirements. *Remote Sensing of Environment*, *115*(11), 2753–2775. https://doi.org/10.1016/j.rse.2011.01.024

Harris, N. L., Gibbs, D. A., Baccini, A., Birdsey, R. A., de Bruin, S., Farina, M., Fatoyinbo, L., Hansen, M. C., Herold, M., Houghton, R. A., Potapov, P. V., Suarez, D. R., Roman-Cuesta, R. M., Saatchi, S. S., Slay, C. M., Turubanova, S. A., & Tyukavina, A. (2021). Global maps of twenty-first century forest carbon fluxes. *Nature Climate Change*, *11*(3), Article 3. https://doi.org/10.1038/s41558-020-00976-6

Harper, K.L.; Lamarche, C.; Hartley, A.; Peylin, P.; Ottlé, C.; Bastrikov, V.; San Martín, R.; Bohnenstengel, S.I.; Kirches, G.; Boettcher, M.; Shevchuk, R.; Brockmann, C.; Defourny, P. (2023): ESA Land Cover Climate Change Initiative (Land_Cover_cci): Global Plant Functional Types (PFT)[Dataset], v2.0.8. NERC EDS Centre for Environmental Data Analysis, *26 January 2023*. doi:10.5285/26a0f46c95ee4c29b5c650b129aab788. https://dx.doi.org/10.5285/26a0f46c95ee4c29b5c650b129aab788

Hese, S., Lucht, W., Schmullius, C., Barnsley, M., Dubayah, R., Knorr, D., Neumann, K., Riedel, T., & Schröter, K. (2005). Global biomass mapping for an improved understanding of the CO2 balance—The Earth observation mission Carbon-3D. *Remote Sensing of Environment*, *94*(1), 94–104. https://doi.org/10.1016/j.rse.2004.09.006

Houghton, R. A., Hall, F., & Goetz, S. J. (2009). Importance of biomass in the global carbon cycle. *Journal of Geophysical Research: Biogeosciences*, *114*(G2). https://doi.org/10.1029/2009JG000935

Hu, T., Su, Y., Xue, B., Liu, J., Zhao, X., Fang, J., & Guo, Q. (2016). Mapping Global Forest Aboveground Biomass with Spaceborne LiDAR, Optical Imagery, and Forest Inventory Data. *Remote Sensing*, *8*(7), Article 7. https://doi.org/10.3390/rs8070565

Hyde, P., Dubayah, R., Peterson, B., Blair, J., Hofton, M., Hunsaker, C., Knox, R., & Walker, W. (2005). Mapping forest structure for wildlife habitat analysis using waveform lidar:

624 Validation of montane ecosystems. *Remote Sensing of Environment*, *96*(3–4), 427–437.
625 https://doi.org/10.1016/j.rse.2005.03.005
626 Jiang, F., Deng, M., Tang, J., Fu, L., & Sun, H. (2022). Integrating spaceborne LiDAR and
627 Sentinel-2 images to estimate forest aboveground biomass in Northern China. *Carbon*
628 *Balance and Management*, *17*(1), 12. https://doi.org/10.1186/s13021-022-00212-y
629 Joshi, N., Mitchard, E. T. A., Brolly, M., Schumacher, J., Fernández-Landa, A., Johannsen, V.
630 K., Marchamalo, M., & Fensholt, R. (2017). Understanding 'saturation' of radar signals
631 over forests. *Scientific Reports*, *7*(1), 3505. https://doi.org/10.1038/s41598-017-03469-3
632 Lefsky, M. A., Cohen, W. B., Harding, D. J., Parker, G. G., Acker, S. A., & Gower, S. T. (2002).
633 Lidar Remote Sensing of Above-Ground Biomass in Three Biomes. *Global Ecology and*
634 *Biogeography*, *11*(5), 393–399.
635 Li, Y., Li, M., Li, C., & Liu, Z. (2020). Forest aboveground biomass estimation using Landsat 8
636 and Sentinel-1A data with machine learning algorithms. *Scientific Reports*, *10*(1), Article
637 1. https://doi.org/10.1038/s41598-020-67024-3
638 Manu, R., Corre, M. D., Aleeje, A., Mwanjalolo, M. J. G., Babweteera, F., Veldkamp, E., & van
639 Straaten, O. (2022). Responses of tree growth and biomass production to nutrient
640 addition in a semi-deciduous tropical forest in Africa. *Ecology*, *103*(6), e3659.
641 https://doi.org/10.1002/ecy.3659
642 Popescu, S. C. (2007). Estimating biomass of individual pine trees using airborne lidar. *Biomass*
643 *and Bioenergy*, *31*(9), 646–655. https://doi.org/10.1016/j.biombioe.2007.06.022
644 Santoro, M., Cartus, O., Mermoz, S., Bouvet, A., Le Toan, T., Carvalhais, N., Rozendaal, D.,
645 Herold, M., Avitabile, V., Quegan, S., Carreiras, J., Rauste, Y., Balzter, H., Schmullius,
646 C., Seifert, F.M., 2018, GlobBiomass global above-ground biomass and growing stock
647 volume datasets. [Dataset] http://globbiomass.org/products/global-mapping
648 Santoro, M., & Cartus, O. (2018). Research Pathways of Forest Above-Ground Biomass
649 Estimation Based on SAR Backscatter and Interferometric SAR Observations. *Remote*
650 *Sensing*, *10*(4), Article 4. https://doi.org/10.3390/rs10040608
651 Santoro, M., & Cartus, O. (2021). *ESA Biomass Climate Change Initiative (Biomass_cci):*
652 *Global datasets of forest above-ground biomass for the years 2010, 2017, and 2018, v3*.
653 [Dataset] Centre for Environmental Data Analysis (CEDA).
654 https://doi.org/10.5285/84403D09CEF3485883158F4DF2989B0C

Santoro, M., Cartus, O., Carvalhais, N., Rozendaal, D. M. A., Avitabile, V., Araza, A., de Bruin, S., Herold, M., Quegan, S., Rodríguez-Veiga, P., Balzter, H., Carreiras, J., Schepaschenko, D., Korets, M., Shimada, M., Itoh, T., Moreno Martínez, Á., Cavlovic, J., Cazzolla Gatti, R., … Willcock, S. (2021). The global forest above-ground biomass pool for 2010 estimated from high-resolution satellite observations. *Earth System Science Data*, *13*(8), 3927–3950. https://doi.org/10.5194/essd-13-3927-2021

Sitch, S., Friedlingstein, P., Gruber, N., Jones, S. D., Murray-Tortarolo, G., Ahlström, A., Doney, S. C., Graven, H., Heinze, C., Huntingford, C., Levis, S., Levy, P. E., Lomas, M., Poulter, B., Viovy, N., Zaehle, S., Zeng, N., Arneth, A., Bonan, G., … Myneni, R. (2015). Recent trends and drivers of regional sources and sinks of carbon dioxide. *Biogeosciences*, *12*(3), 653–679. https://doi.org/10.5194/bg-12-653-2015

Spawn, S. A., Sullivan, C. C., Lark, T. J., & Gibbs, H. K. (2020). Harmonized global maps of above and belowground biomass carbon density in the year 2010. *Scientific Data*, *7*(1), Article 1. https://doi.org/10.1038/s41597-020-0444-4

Spawn, S.A., and H.K. Gibbs. 2020. Global Aboveground and Belowground Biomass Carbon Density Maps for the Year 2010. [Dataset] ORNL DAAC, Oak Ridge, Tennessee, USA. https://doi.org/10.3334/ORNLDAAC/1763

Su, H., Shen, W., Wang, J., Ali, A., & Li, M. (2020). Machine learning and geostatistical approaches for estimating aboveground biomass in Chinese subtropical forests. *Forest Ecosystems*, *7*(1), 64. https://doi.org/10.1186/s40663-020-00276-7

Treuhaft, R. N., Chapman, B. D., dos Santos, J. R., Gonçalves, F. G., Dutra, L. V., Graça, P. M. L. A., & Drake, J. B. (2009). Vegetation profiles in tropical forests from multibaseline interferometric synthetic aperture radar, field, and lidar measurements. *Journal of Geophysical Research: Atmospheres*, *114*(D23). https://doi.org/10.1029/2008JD011674

TRENDY. (2021). Trends in the land carbon cycle. [Dataset] https://globalcarbonbudgetdata.org/closed-access-requests.html

USGCRP. (2018). *Second State of the Carbon Cycle Report* (pp. 1–470). U.S. Global Change Research Program, Washington, DC. https://carbon2018.globalchange.govhttps://carbon2018.globalchange.gov/chapter/9

Woodhouse, I. H., Mitchard, E. T. A., Brolly, M., Maniatis, D., & Ryan, C. M. (2012). Radar backscatter is not a “direct measure” of forest biomass. *Nature Climate Change*, *2*(8),

556–557. https://doi.org/10.1038/nclimate1601

Xiao, J., Chevallier, F., Gomez, C., Guanter, L., Hicke, J. A., Huete, A. R., Ichii, K., Ni, W., Pang, Y., Rahman, A. F., Sun, G., Yuan, W., Zhang, L., & Zhang, X. (2019). Remote sensing of the terrestrial carbon cycle: A review of advances over 50 years. *Remote Sensing of Environment*, *233*, 111383. https://doi.org/10.1016/j.rse.2019.111383

Xue, B.-L., Guo, Q., Hu, T., Xiao, J., Yang, Y., Wang, G., Tao, S., Su, Y., Liu, J., & Zhao, X. (2017). Global patterns of woody residence time and its influence on model simulation of aboveground biomass. *Global Biogeochemical Cycles*, *31*(5), 821–835. https://doi.org/10.1002/2016GB005557

Yang, H., Ciais, P., Santoro, M., Huang, Y., Li, W., Wang, Y., Bastos, A., Goll, D., Arneth, A., Anthoni, P., Arora, V. K., Friedlingstein, P., Harverd, V., Joetzjer, E., Kautz, M., Lienert, S., Nabel, J. E. M. S., O'Sullivan, M., Sitch, S., … Zhu, D. (2020). Comparison of forest above-ground biomass from dynamic global vegetation models with spatially explicit remotely sensed observation-based estimates. *Global Change Biology*, *26*(7), 3997–4012. https://doi.org/10.1111/gcb.15117

Yu, L., Fan, L., Ciais, P., Xiao, J., Frappart, F., Sitch, S., Chen, J., Xiao, X., Fensholt, R., Chang, Z., Fang, H., Li, X., Cui, T., Ma, M., & Wigneron, J.-P. (2024). Forest degradation contributes more to carbon loss than forest cover loss in North American boreal forests. *International Journal of Applied Earth Observation and Geoinformation*, *128*, 103729. https://doi.org/10.1016/j.jag.2024.103729

Zhao, P., Lu, D., Wang, G., Wu, C., Huang, Y., & Yu, S. (2016). Examining Spectral Reflectance Saturation in Landsat Imagery and Corresponding Solutions to Improve Forest Aboveground Biomass Estimation. *Remote Sensing*, *8*(6), Article 6. https://doi.org/10.3390/rs8060469

Zhu, K., Zhang, J., Niu, S., Chu, C., & Luo, Y. (2018). Limits to growth of forest biomass carbon sink under climate change. *Nature Communications*, *9*(1), Article 1. https://doi.org/10.1038/s41467-018-05132-5